Synthetic Metals 213 (2016) 78–87

Contents lists available at ScienceDirect

Synthetic Metals

journal homepage: www.elsevier.com/locate/synmet

A comparative study of one and two dimensional π-conjugated systems

Ana E. Torres, Reyes Flores, Serguei Fomine*

Instituto de Investigaciones en Materiales, Universidad Nacional Autónoma de México, Apartado Postal 70-360, CU, Coyoacán, Mexico, DF 04510, Mexico

ARTICLE INFO

Article history:
Received 13 November 2015
Accepted 7 January 2016

Keywords:
Graphene
DFT
Restricted active space
Multiconfigurational
Polyacetylene
Porous graphene

ABSTRACT

The comparative study of one (**1D**) and two dimensional (**2D**) π-conjugated systems has been carried out at D3 dispersion corrected B3LYP and restricted active space (RAS) levels of theory using oligomer approach. Two sets of systems differeing by the connection density have been studied. The first one is poly-*m*-phenylene (**1D-PMP**) and the corresponding **2D** analogue, porous graphene (**2D-PMP**). The second one is *trans*-polyacetylene (**1D-PA**) and graphene nanoflakes(**2D-PA**). Both **1D**- and **2D-PMP** have closed shell singlet ground state. **2D-PMP** systems have higher ionization potential (IP), electron affinity (EA) and lower band gap (E_g) than **1D-PMP** of the similar size. The ground state of **1D-PA** is a single reference singlet while the nature of **2D-PA** ground state depends strongly on the size. The small members of **2D-PA** series have singlet ground states (single- or multireferencial). The larger members have single reference high spin ground states with number of unpaired electrons increasing with their size and reaching 12 for the largest member of **2D-PA** series according to both B3LYP and RAS methods. Similar to **PMP,** E_g decreases with size more rapidly for **2D-PA** than for **1D-PA** and ionization potentials are higher for **2D-PA** of the similar size.Unlike **1D-PMP** and **2D-PMP** the electron affinities of **1D-PA** are consistently higher then these of **2D-PA**.

1. Introduction

In 1964 Little [1] proposed that replacing some of the hydrogen atoms in polyacetylene (PA) by specifically designed substituents would create a high temperature superconductor. The hope of a room temperature superconductor has not yet been fulfilled, however, this idea promoted the interest in π-conjugated polymers culminating in the discovery that their conductivity increases notably upon doping [2,3]. Many research groups, in both industry and academy were exploring the field of π-conjugated systems ranging from small molecules and fullerenes to polymers and nanotubes revealing their unique semiconducting and optical properties, paving the way for the field of photonics and plastic electronics [4,5].

Nowadays, π-conjugated polymers and structurally similar carbon nanotubes are the mainstream of organic electronics. They can be considered as one-dimensional (**1D**) systems. However, two dimensional (**2D**) structures have been becoming increasingly important since the discovery of graphene in 2004 [6]. There is a fundamental difference in the electronic structure between **1D** and **2D** conjugated systems due to the Peierls instability which is inherent for **1D** systems [7]. The Peierls distortion opens up a gap which is proportional to the bond length alternation in the conjugated polymers [8]. It can, however, be manipulated to some extent by the appropriate choice of the repeat units, the substituents or the alternating electron donating and electron withdrawing groups in the polymer main chain [9].

The electronic structure of **1D** conjugated systems is a well-established area. A notable band gap in **1D** conjugated systems leads mostly to the single reference ground state, therefore, DFT can widely be used as a research tool for these systems. However, **2D** conjugated systems are much less explored. The first attempts to predict electronic properties of **2D** conjugated systems are dated back to 1980–1990s [10–12]

The discovery of graphene unleashed the interest in the electronic structure of **2D** organic conjugated systems. Thus, Deleuze et al. studied graphene nanoribbons using the formalism of crystalline orbitals [13]. They found that for singlet states, symmetry-breakings in spin-densities are necessarily the outcome of a too approximate treatment of static and dynamic electron correlation in single-determinant approaches, and is thus nothing else than a methodological artefact. Rayne and Forest [14,15] studied polyacenes and rectangular graphene nanoribbons assuming a closed shell singlet ground state. They concluded that graphene [**mxn**] nanoribbons have closed shell ground state with

* Corresponding author.
E-mail address: fomine@servidor.unam.mx (S. Fomine).

http://dx.doi.org/10.1016/j.synthmet.2016.01.005
0379-6779/

vanishing S_0-T_1 energy gap at polymeric limit ($\mathbf{m} \rightarrow \infty$ and/or $\mathbf{n} \rightarrow \infty$). In recent papers [16,17] a conclusion has been reached that graphene nanoribbons, both pristine and nitrogen doped, present strong multiradicalic character, D2 diagnostic confirms multiconfigurational character of the ground state of these systems. A similar situation holds for large fused aromatic hydrocarbons [17].

The differences between **1D** and **2D** HOMO-LUMO gaps (HLG) evolution have recently been studied by Gutsler and Perepichka [18] at hybrid DFT level. The results show that the HLG of **2D** conjugated polymers is always smaller than that of their **1D** counterpart, depending critically on the connectivity between the repeat units in **2D** systems. The contraction of the HLG follows a different convergence behaviour: while in **1D** the HLG reduction becomes smaller for each additional repeat unit, in **2D** the HLG contraction becomes faster for increasing oligomer size. The authors suggested that it can be related to the number of the connections that scales linearly with the oligomer length in **1D** but superlinearly in **2D** [18].

The aim of this manuscript is to provide a detailed comparative analysis of the electronic properties of **1D** and **2D** conjugated systems. It is well known that single reference methods failed to accurately describe large fused aromatic hydrocarbons and nanoribbons due to multireference ground states of these systems [16,17] thus, resulting in too low ionization potentials (IP's), electron affinities (EA's) and HLG's. Therefore, one of the important tasks is also to find the limits of applicability of single reference methods for **2D** systems.

2. Computational details

All geometry optimizations have been carried out using D3 (BJ) dispersion corrected [19] B3LYP functional as implemented in Turbomole 6.6 [20]. Dunning's correlated consistent cc-pVDZ basis set [21] was applied for all except for restricted active space calculations (RAS) where 6–31G(d) basis set has been used [22]. The geometries of all the structures have been optimized for singlets, triplets and multiplets using restricted and unrestricted methods, respectively. When triplet instability has been detected for the closed shell singlet state, the geometry was reoptimized using broken symmetry (BS) unrestricted method (UB3LYP). BS-DFT can deal with systems which show moderate multiconfiguration character. Thus, experimental singlet—triplet splitting of trimethylenemethane is of 16.1 kcal/mol [23]. However, the restricted B3LYP/cc-pVDZ model gives inacceptable 42.6 kcal/mol. BS-UB3LYP/cc-pVDZ delivers reasonable 12.1 kcal/mol. It must be mentioned that B3LYP functional benefits greatly from dispersion correction, especially D3 (BJ) flavour, improving geometry optimization results and energetics. [24] Without this correction B3LYP produces meaningless results for large molecules.

The hole reorganization energies (λ_+) of GNRs were estimated as follows:

$$\lambda_+ = (E_n^+ - E_n) + (E_+^n - E_+)$$

where E_n and E_+ are the energies of the neutral and cationic species in their lowest energy geometries, while E_n^+ and E_+^n are the energies of the neutral and cationic species with the geometries of the cationic and neutral species, respectively. The electron reorganization energy (λ_-) is defined similarly:

$$\lambda_- = (E_n^- - E_n) + (E_-^n - E_-)$$

In this case, E_n and E_- are the energies of the neutral and the anionic species in their lowest energy geometries, while E_n^- and E_-^n are the energies of the neutral and anionic species with the geometries of the anionic and neutral species, respectively.

To evaluate the multiconfigurational character of the studied systems, RAS single point energy calculations were carried out for the systems that showed triplet instability of the closed shell singlet state. B3LYP optimized structures of the corresponding multiplicity were used and the active space consisting of 20 electrons and 20 orbitals there was applied. The 20,20 active space was the largest practical active space. For all atoms the 6–31 G (d) basis set was used. These calculations were carried out with Gaussian 09 rev. D.01 code [25]. In the RAS model, the active space is divided into three distinct subspaces: RAS1, RAS2, and RAS3. The RAS2 subspace is identical to the active space in a complete active space calculation, the RAS1 and RAS3 subspaces, on the other hand, subject to the restriction that a maximum number of excitations may occur from RAS1, which otherwise contains only doubly occupied orbitals, and a maximum number of excitations may occur into RAS3, which otherwise contains only empty orbitals. In RAS calculations, the RAS2 space consisted of 4 electrons distributed in 4 orbitals for singlets and 6 electrons in 6 orbitals for triplets, increasing by 2 electrons and 2 orbitals for each 2 extra unpaired electrons for high spin states. Therefore, RAS1 involved 8 and 7 double occupied orbitals in singlets and triplets, respectively. RAS3 included 7 virtual orbitals for triplets and 8 for singlets. Up to double excitations from RAS1 into RAS3 were considered. As shown [26] the inclusion of double excitations in RAS allows to reproduce well IP's and EA's of oligomeric unsaturated hydrocarbons.

The band gaps (E_g) of **1D** and **2D** systems have been estimated as the lowest excitation energy from the corresponding ground state which is not necessarily singlet state using time dependent (TD) implementation of M06-2X functional [27]. TD-M06-2X reproduces very well the absorption spectra of organic dyes. [28–30] The high amount of HF exchange (54%) make this functional relatively insensible to low overlap excitations. TD-M06-2X/cc-pVDZ//B3LYP-D3(BJ)/cc-pVDZ model reproduces well the lowest excitation energy of recently synthesized aza analogue of nanocene: octaazanonacene-8,19-dione [31] (1.95 eV *vs* 1.82 eV (exp)). In the case of unstable singlet closed shell solution for the reference state, the BS unrestricted singlet solution was used.

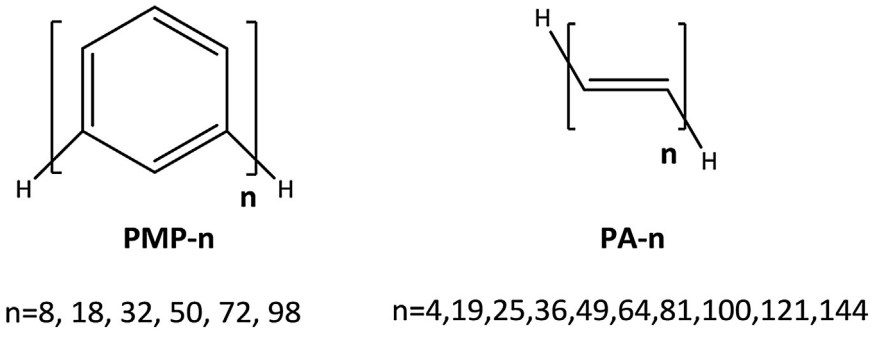

Fig. 1. Structures of **1D-PMP** and **1D-PA**.

Table 1
HOMO-LUMO gaps (HLG), adiabatic ionization potentials (IP), electron affinities (EA), hole (λ_+) and electron (λ_-) reorganization energies of **1D-** and **2D-PMP** estimated at B3LYP-D3(bj)/cc-pVDZ level, S_0-S_1 excitation energies (E_g) estimated at TD-M06-2X/cc-pVDZ level (*eV*).

Molecule	HLG	E_g	IP	EA	λ_+	λ_-
1D-PMP-8	4.52 (4.59)[a]	4.47	6.73	0.52	0.0021	0.0032
2D-PMP-8	4.18 (4.28)[a]	4.26	6.75	0.64	0.0026	0.0031
1D-PMP-18	4.47 (4.55)[a]	4.45	6.41	0.91	0.0012	0.0014
2D-PMP-18	4.02 (4.14)[a]	4.11	6.49	1.08	0.0023	0.0015
1D-PMP-32	4.46 (4.55)[a]	4.45	6.36	1.09	0.0007	0.0008
2D-PMP-32	3.94 (4.07)[a]	4.07	6.37	1.33	0.0005	0.0009
1D-PMP-50	4.46	4.45	6.16	1.19	0.0005	0.0005
2D-PMP-50	3.88	4.05	6.31	1.49	0.0003	0.0006
1D-PMP-72	4.46	4.45	6.10	1.25	0.0003	0.0003
2D-PMP-72	3.84	4.04	6.22	1.60	0.0003	0.0003
1D-PMP-98	4.45	4.45	6.07	1.30	0.0004	0.0004
2D-PMP-98	3.81	4.03	6.19	1.70	0.0003	0.0003

[a] B3LYP/6-31G(d) level [18].

The chemical structures of studied systems are shown in Fig. 1. We have selected 2 systems, graphene like structures and porous graphene. These structures are denoted as **2D-PA-n** and **2D-PMP-n**, respectively. The **1D** analogue of graphene is *trans*-polyacetylene (**PA**), while the **1D** analogue of porous graphene is poly-*m*-phenylene (**PMP**). ***n*** Stands for the number of formal double bonds in **PA** and **2D-PA** while in **PMP** and **2D-PMP** ***n*** represents the number of phenyl rings. All 4 systems **PA** [32]. Graphene nanoflakes [6],**PMP** [33] and porous graphene [34] are experimentally available. Although both graphene and porous graphene are **2D** systems the number of the connections between carbons are different, being higher in graphene.

As it has been noted in Ref. [18] the dimensionality and the number of the connections between carbons atoms of a conjugated system strongly affects HLG. This research is aimed at exploring the effect of the dimensionality on the electronic structure of conjugated systems.

3. Results and discussion

3.1. 1D- and 2D-PMP

Table 1 shows E_g's, adiabatic IP's, EA's and reorganization energies for **1D-** and **2D-PMP** systems. Their structures are shown in Figs. 1–3.

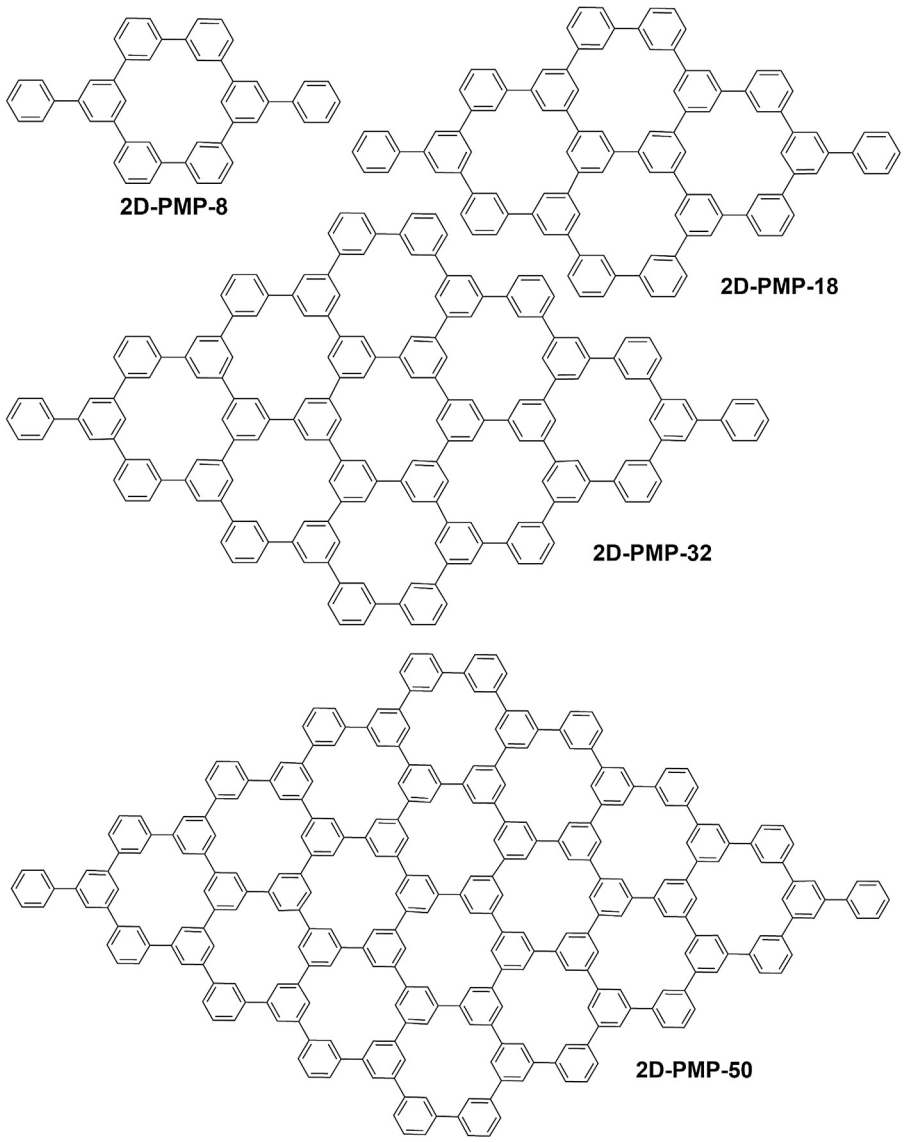

Fig. 2. Structures of **2D-PMP**.

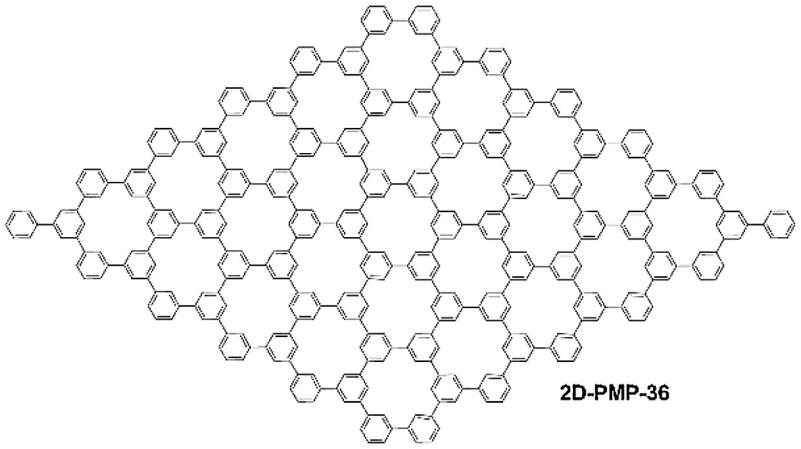

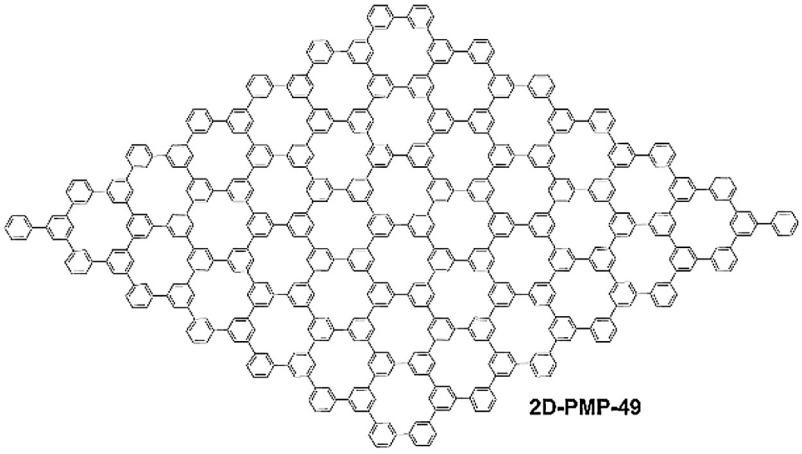

Fig. 3. Structures of **2D-PMP**.

Table 2
HOMO-LUMO gaps (HLG), adiabatic ionization potentials (IP), electron affinities (EA), hole (λ_+) and electron (λ_-) reorganization energies of **1D** and **2D-PA** estimated at B3LYP-D3/cc-pVDZ level, lowest excitation energies (E_g) estimated at TD-B3LYP/cc-pVDZ level (*eV*), triplet-singlet energy gap (E_{t-s}) (kcal/mol).

Molecule	HLG	E_g	IP	EA	λ_+	λ_-	E_{t-s}
1D-PA-4	3.76 (3.80)[a]	4.39	7.05	0.22	0.0100	0.0160	35.52
2D- PA-4	3.73 (3.80)[a]	4.54	7.24	0.04	0.0076	0.0129	31.39
1D- PA-9	2.34 (2.30)[a]	2.86	5.75	1.49	0.0120	0.013	17.68
2D- PA-9	1.91 (1.90)[a]	1.95	6.12	1.25	0.010	0.0121	6.61[b]
1D-PA-16	1.75 (1.70)[a]	2.19	5.11	2.11	0.0110	0.0130	10.19
2D-PA-16	0.96 (0.90)[a]	1.35	5.97	1.49	0.0048	0.0044	2.96 [b]
1D-PA-25	1.48 (1.30)[a]	1.89	4.78	2.44	0.0127	0.0130	6.35
2D-PA-25	0.48 (0.50)[a]	1.76	5.78	1.57	0.0048	0.0020	6.53[b]
1D-PA-36	1.34	1.75	4.59	2.62	0.0009	0.0148	4.06
2D-PA-36	0.26	0.96	5.10	2.25	0.0024	0.0028	−23.22[b,c]
1D-PA-49	1.28	1.68	4.50	2.71	0.0175	0.0174	2.89 [b]
2D-PA-49	0.19	0.84	4.94	2.59	0.0017	0.0019	−12.95 [b,d]
1D-PA-64	1.24	1.64	4.46	2.75	0.0169	0.0167	2.20[b]
2D-PA-64	0.10	0.26	4.76	2.67[c)]	0.0373	0.0093	−12.70[b,e]
1D-PA-81	1.22	1.62	4.44	2.77	0.0071	0.010	1.94 [b]
2D-PA-81	0.12	0.65	4.81	2.61	0.0012	0.0020	−16.58 [b,f]
1D-PA-100	1.20	1.60	4.43	2.77	0.0351	0.0347	1.82 [b]
2D-PA-100	0.21	0.64	4.62	2.55	0.0012	0.0020	−13.4 [b,g]
1D-PA-121	1.20	1.60	4.31	2.92	0.0273	0.0419	1.54 [b]
2D-PA-121	–	0.53	4.73	2.90	0.0008	0.0015	−20.6[b,h]
1D-PA-144	1.15	1.57	4.35	2.85	0.011	0.0137	5.45[b]
2D-PA-144	–	0.53	4.58	2.84	0.0009	0.0016	−14.28[b,i]

[a] B3LYP/6-31G(d) level [18].
[b] Broken symmetry singlet solution.
[c] Quintet ground state, 3.31 kcal/mol below triplet.
[d] Septet ground state, 3.12 kcal/mol below triplet.
[e] Septet ground state, 10.8 kcal/mol below triplet.
[f] Nonet ground state, 11.86 kcal/mol below triplet.
[g] Undecaplet ground state, 13.2 kcal/mol below triplet.
[h] Undecaplet ground state, 18.8 kcal/mol below triplet.
[i] Tridecaplet ground state, 19.9 kcal/mol below triplet.

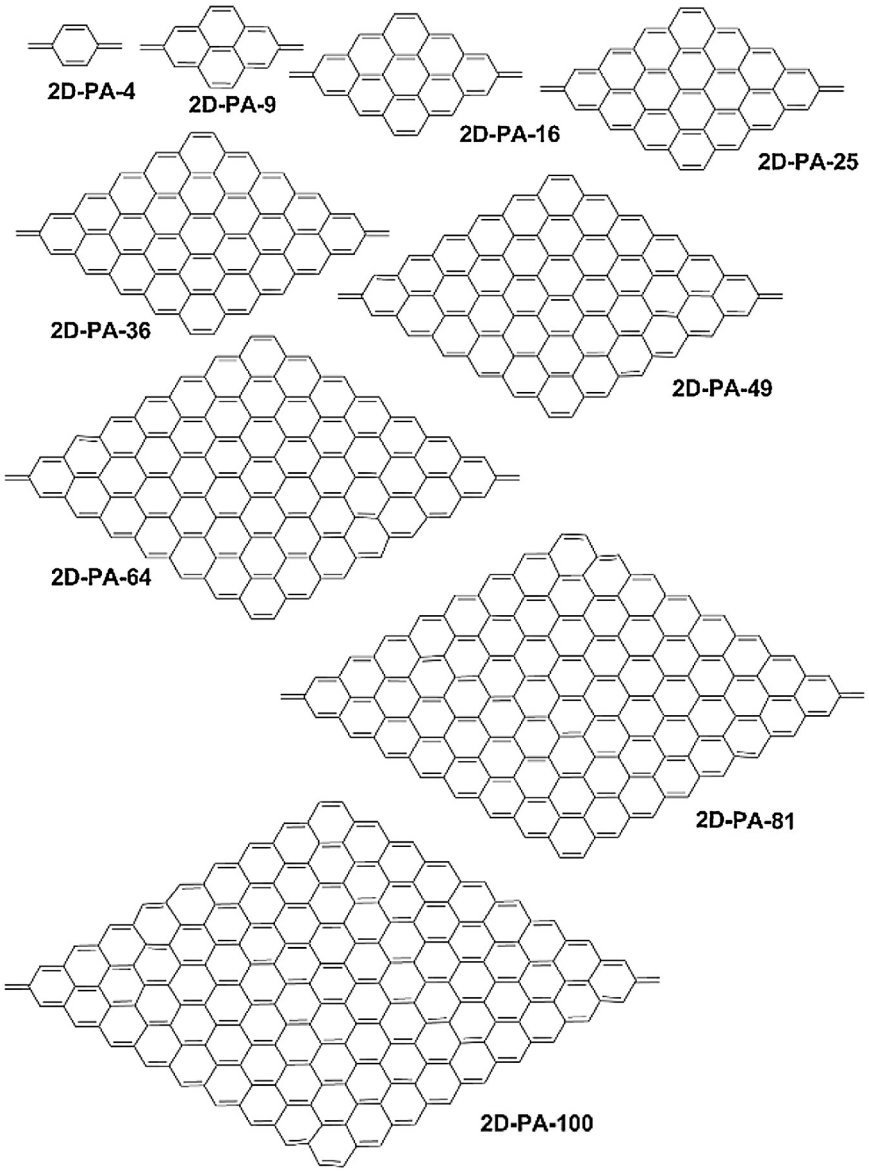

Fig. 4. Structures of 2D-PA.

The band gaps were estimated by two methods, as HOMO-LUMO difference at B3LYP-D3/cc-pVDZ level and as S_0-S_1 excitation energies estimated at TD-M06-2X/cc-pVDZ level of theory. Additionally the E_g values based on HOMO-LUMO energy differences taken from reference 18 are listed for some of the **1D-** and **2D-PMP** systems.

Restricted solutions were stable for all **1D** and **2D** systems regardless on their size, demonstrating single reference nature of the ground state independent on dimensionality. As seen HLG and S_0-S_1 excitation energies at TD-DFT level agree reasonably with each other. E_g's of **2D** systems are notably lower than those for **1D** in agreement with [18]. The difference between E_g's of **1D** and **2D** systems increases with their size. As seen, E_g does not decrease for **1D-PMP** for structures larger than **1D-PMP-18**, which is related with the restriction imposed for **1D** systems by Peierls theorem, for **2D-PMP** E_g drops constantly with the size of the system. Thus, the difference between **1D** and **2D-PMP-98** reaches more than 0.4 eV.

The IP's and EA's listed in Table 1 show unexpected behaviour. For both **1D** and **2D** systems IP's decrease and EA's increase with the size of the molecule as could be expected for conjugated polymers where extended pi-conjugated fragments stabilize better both cations and anions. However, IP's of **1D-PMP** are always lower compared to **2D-PMP** and this difference increases with size from 0.02 to 0.12 eV. On the other hand, EA's are higher for **2D-PMP** and the difference increase with size from 0.12 to 0.40 eV (Table 1). The explanation of this behaviour is related with the different C/H ratio in **1D** and **2D** systems. The sp^2 carbon is notably more electronegative compared to hydrogen and the C/H ratio is higher for **2D** systems compared to **1D**.

Moreover, C/H ratio increases with the size of **2D** structures and does not change for **1D**. Therefore, the molecular electronegativity increases with the size for bidimensional molecules and does not change for **1D**. This results in higher IP's and EA's for **2D** systems, also increasing the difference between these properties (IP's and EA's) for **1D** and **2D-PMPs** with the size of the systems.

An important point in understanding conductivity of organic conjugated polymers is to characterize structural factors essential in the charge transfer rates. Thus, it has been demonstrated that the solid-state hole mobility in arylamines is related to the internal reorganization energy λ [35–37]. It is very well documented that there is a linear correlation between λ and 1/**n** for conjugated

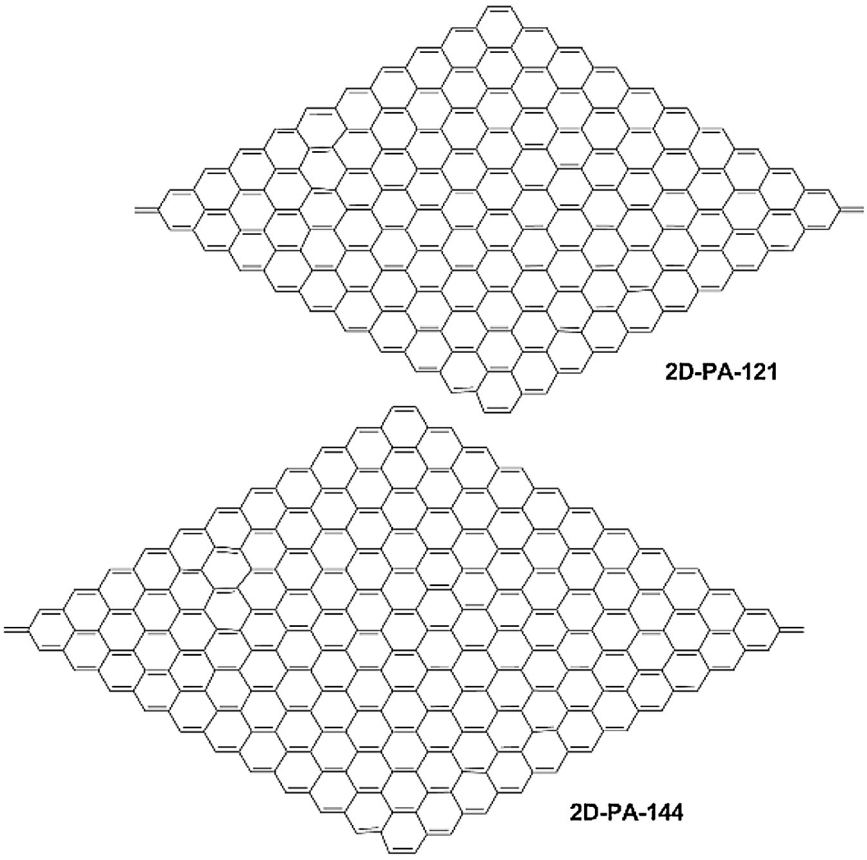

Fig. 5. Structures of **2D-PA**.

polymers such as for polythiophene and polyselenophene, where **n** is the number of repeat units [38].

As could be seen from Table 1, the reorganization energies show the same trend for **1D-PMP**; R^2 for the linear correlation between λ and 1/**n** are of 0.981 and 0.995 for the electron and the hole reorganization energies, respectively. For the electron reorganization energy of **2D-PMP** R^2 is 0.993, while for the hole reorganization energies of **2D-PMP** R^2 is only 0.673. For the largest members of **1D** and **2D-PMP** families λ for both electron and hole transport are similar being around 0.0003- 0.0004 eV, very close to zero.

Fig. 6 shows HOMO's of the cation and anion radicals for the smallest and the largest members of **1D-** and **2D-PMP** which could be interpreted as polaron delocalization.

As seen from Fig. 6 the delocalization patterns of polaron cations and polaron anions are different, however, one can observe the similarity for polaron anion delocalization patterns for **1D** and **2D** systems. The delocalization of polaron anions involves the entire molecule for both **1D** and **2D** systems while most of the polaron cations are localized on the edges of the molecules for **1D-PMP** and show different patterns for different **2D-PMP** molecules. The uniform delocalization of polaron anions contributes to high R^2 values for both **1D** and **2D-PMP's**. On the other hand, the localization of polaron cations leads, especially for **2D** case, in low R^2.

3.2. 1D- and 2D-PA

The electronic structure of **2D-PA's** differs dramatically from that of **2D-PMP** due to higher connection density (Table 2), Figs. 1, 4, 5). Unlike **1D** and **2D-PMP**, the closed shell solution for the singlet state is stable only for the first member of **2D-PA** series, while for the **1D-PA's** the instability of closed shell singlet solution is detected only for **1D-PA-49** and larger systems, indicating possible multireference character of the singlet states of almost all **2D-PA's** and largest members of **1D-PA** series. As a result, HLG's may not be reliable for the systems with heavily multiconfigurational character. As seen HLG for **1D-PA-144**, the largest **1D-PA**, is significantly lower than the experimental band gap of 1.4 eV obtained for *trans*-**PA** [39] TD-M06-2X method produces much better results. Both HLG and TD-M06-2X results, however, agree that E_g is always smaller for **2D-** compared to **1D-PA's** which is also in accordance with [18]. Although there is a reasonable agreement between HLG and TD-M06-2X results for **1D-PA** and smallest members of **2D-PA** series, for medium and high members of **2D-PA** series HLG and TD-M06-2X results sometimes differ by more than 1 eV (Table 2). For **2D-PA-121** and **2D-PA-144** the closed shell solution was impossible to obtain due to convergence problems and therefore HLG's were unavailable for these systems.

It came as a surprise that, starting from **2D-PA-36** the ground states for the members of **2D-PA** series were not singlets anymore but high spin states (Table 2). The number of unpaired electrons in the ground state increases from 4 for **2D-PA-36** to 12 for **2D-PA-144**.

The energies of the high spin states lie well below the BS unrestricted singlet and triplet states. As can be seen from Table 4 the $<S^2>$ expectation values are very close to the theoretical value of S(S + 1) indicating very small spin contamination and, therefore, single reference character of the ground state. This phenomenon has been observed earlier [17]. For fused aromatic hydrocarbons. The higher was the multiplicity of the state the lower was the spin contamination.

It is noteworthy that the high spin ground states for **2D** conjugated systems were predicted back to 1978 [40] using valence bond method. More recently, the high spin ground states were

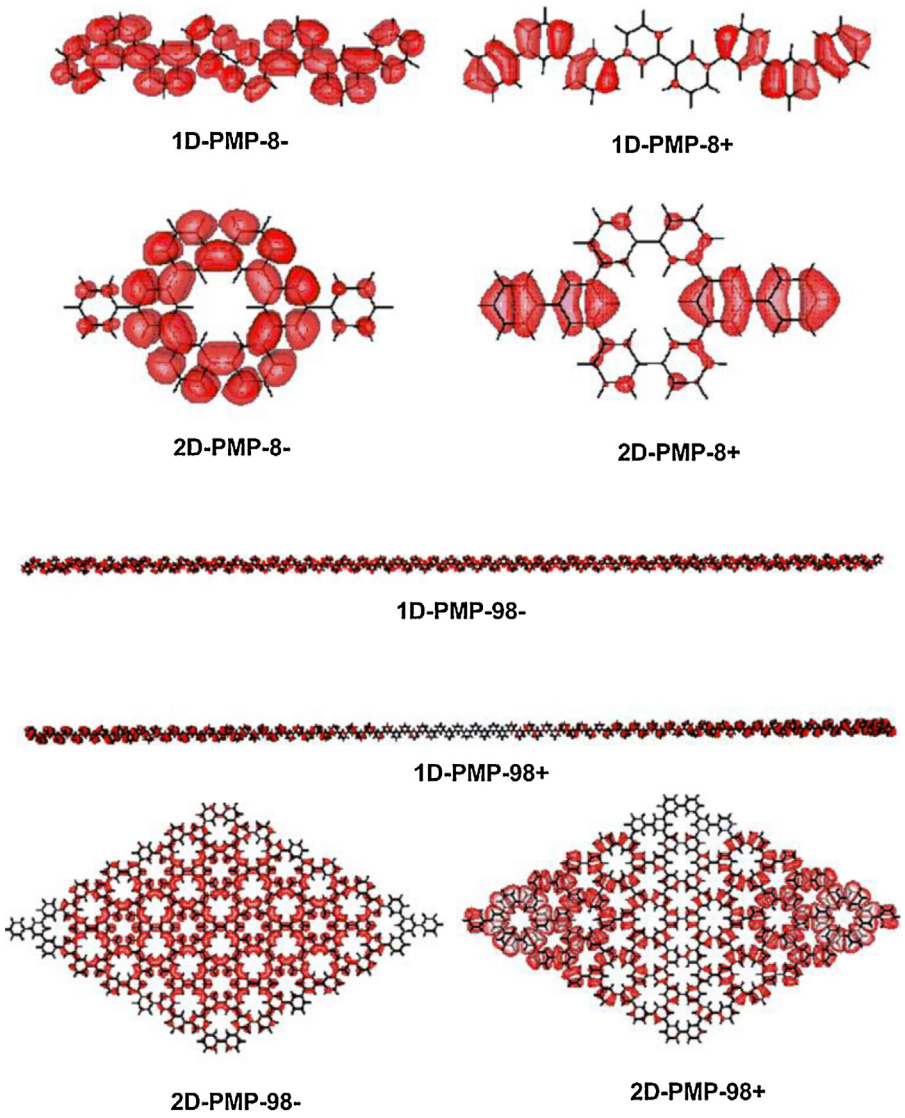

Fig. 6. Polaron delocalization in **1D-** and **2D-PMP**.

confirmed at unrestricted DFT level for various polycyclic hydrocarbons [41,42]. However, in some cases BS unrestricted singlet solutions were the found to be slightly more stable than the corresponding high spin states [43]. In our cases, however, the high spin states were found to be the ground states, the BS singlet solutions were significantly higher in energy (Table 2).

The ground states of the corresponding cation and anion radicals of **2D-PA's** are also high spin states (Table 4). Normally, the ground state of an anion radical has one unpaired electron more and the cation radical has one electron less than the neutral state. The exceptions were the cation radicals of **2D-PA-36** and **64** where it had been found that the ground state had 5 and 7 unpaired electrons, respectively, and anion radical of **2D-PA-49** possessing 5 unpaired electrons in the ground state. Fig. 7 shows the spin density distribution for these **2D-PA** where the high spin states are the ground states.

As seen, in all cases most of the spin density is located in the vicinity of methylene groups and on the edges of the hydrocarbon, independently on the number of the unpaired electrons in the ground state.

The IP's and EA's decrease with the size for both **1D-PA** and **2D-PA** similarly to **1D** and **2D-PMP** (Table 2).

However, unlike **1D** and **2D-PMP** where IP's and EA's of **2D PMP**'s are constantly higher compared to those of **1D-PMP**, EA's of **2D-PA** are lower than those for **1D-PA** while IP's are higher. This might be related with the higher connection density in **2D-PA** compared to **2D-PMP** resulting in higher π—electron density. Therefore, the electron repulsion in anionic **2D-PA** species are notably higher compared to that of **1D-PA**, thus reducing the electron affinity of **2D-PA**'s. Another difference is related to the reorganization energies. As seen from Table 2 there is no correlation whatsoever between the reorganization energies (hole and electrons) and the size of **1D-** and **2D-PA**'s. Since the reorganization energies normally are small (do not exceed a few hundredths of *eV*) the errors in DFT energies induced by spin contamination for medium and large members of **1D** and **2D-PA** series could seriously affect the reorganization energies.

The experimental data for IP of *trans*-PA is 4.7 eV [44]. This is very close to the calculated IP for **1D-PA-121** (4.73 eV, Table 2). Particularly, for the longest **1D-PA-144** the estimated adiabatic IP was found to be slightly lower (4.35 eV) than the experimental data. This could be related to the long length of **1D-PA-144** which probably exceeds the effective conjugated length in **PA** limited by the presence of different kind of defects. Taking this as a reasonable hypothesis it is possible to estimate the average effective

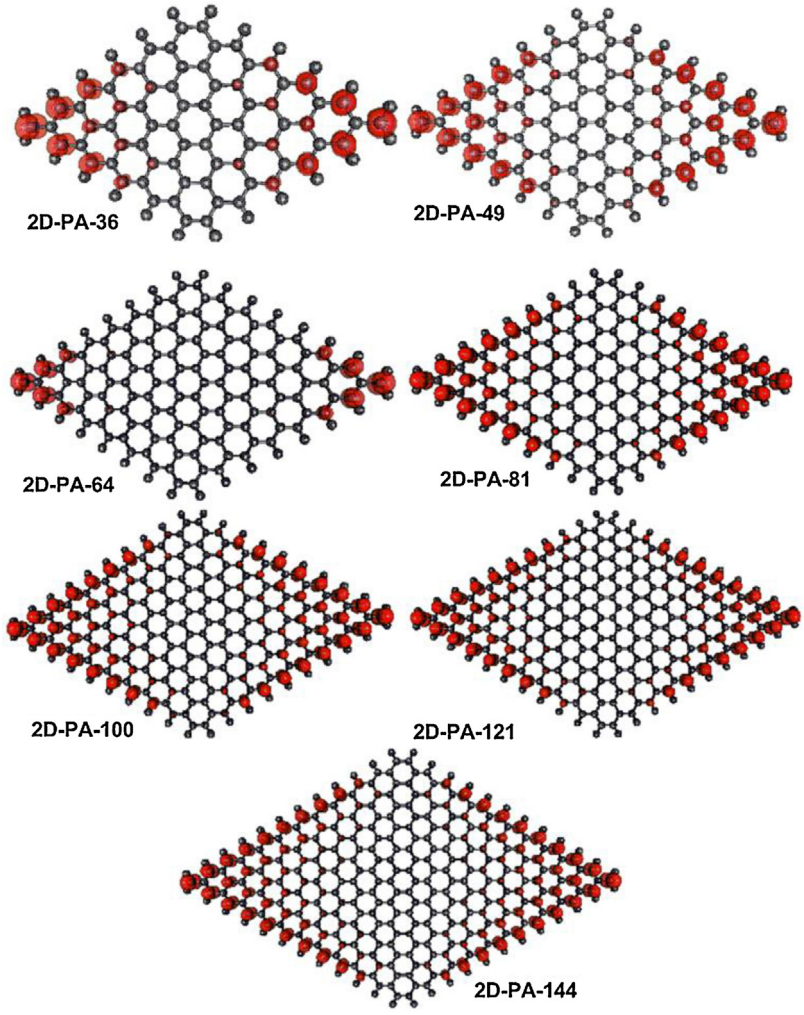

Fig. 7. Spin density distribution in high spin ground states of **2D-PA's**.

conjugation length in PA as about 121 repeat units (the size of **1D-PA-121**).

Table 3 shows the results of RAS calculations for **1D-PA**'s and **2D-PA**'s. We were unable to obtain RAS data for the largest **1D** and **2D-PA-144** molecules in reasonable time, since these **calculations** are extremely computationally **demanding**. As seen all **1D-PA** have mostly single reference ground state in spite of significant spin contamination for large **1D-PA** (Table 4), the squared CI expansion coefficients for the lowest energy configuration exceeds 0.7 for both singlet and triplet states. In the case of **2D-PA**'s only the first member of the series has a single reference ground state while starting from **2D-PA-9** the contribution from the lowest energy configuration drops below 0.5 for the singlet state. For the triplet state this occurs for **2D-PA-36**. Moreover, starting from **2D-PA-81** the lowest energy configuration barely contributes to either the singlet or the triplet state. This means that singlet and triplet states of medium and large members of **2D-PA** series cannot be properly described within the framework of single reference methods like DFT. BS approach partially alleviates this drawback of DFT at the expense of spin contamination. However, the spin contamination becomes very important for these states already for **2D-PA-25** (Table 3) not to mention larger members of **2D-PA** series.

Therefore, the DFT relative energies of the medium and large members of **2D-PA**'s for singlet and triplet states could be unreliable and must be compared with those obtained using

Table 3
Squared CI expansion coefficients for singlet (C^2_s) and triplet (C^2_t) states for the lowest energy configurations in **1D** and **2D PA**'s and triplet – singlet gap (E_{t-s}) using RAS method. Number of electrons out of the valence shell for singlet (N_s) and triplet (N_t) states.

Molecule	E_{t-s}	C^2_s	N_s	C^2_t	N_t
2D- PA-9	22.2	0.71	0.85	0.78	0.25
1D-PA-16	29.2	0.79	0.42	0.72	0.46
2D-PA-16	−5.68	0.44	1.27	0.75	0.45
1D-PA-25	32.5	0.76	0.51	0.68	0.53
2D-PA-25	−10.9	0.31	1.70	0.75	0.51
1D-PA-36	44.9	0.76	0.51	0.70	0.52
2D-PA-36	−18.8[a]	0.18	2.19	0.77[a]	0.34[a]
1D-PA-49	60.7	0.76	0.52	0.72	0.53
2D-PA-49	−23.9	0.15	2.31	0.07	2.09
1D-PA-64	69.4	0.78	0.46	0.72	0.55
2D-PA-64	−50.0[b]	0.11	2.61	0.72[b]	0.38[b]
1D-PA-81	83.9	0.78	0.46	0.71	0.52
2D-PA-81	−75.6	0.00	4.00	0.00	2.28
1D-PA-100	110.7	0.75	0.54	0.74	0.53
2D-PA-100	−83.4[c]	0.00	4.00	0.80[c]	0.29[c]
1D-PA-121	134.3	0.75	0.54	0.73	0.54
2D-PA-121	−105.4[d]	0.00	4.00	0.81[d]	0.31[d]

[a] Quintet ground state, 2.4 kcal/mol below triplet.
[b] Septet ground state, 10.8 kcal/mol below triplet.
[c] Undecaplet ground state, 80.1 kcal/mol below triplet.
[d] Undecaplet ground state, 73.1 kcal/mol below triplet.

Table 4
$<S^2>$ expectation values for 1-D and 2-D PA's for singlet (S), triplet (T) cationic (CAT) and anionic (ANI) states at B3LYP + D3/cc-pVDZ level.

Molecule	S	ANI	CAT	T
1D-PA-4	0	0.77	0.78	2.03
2D- PA-4	0	0.77	0.79	2.00
1D- PA-9	0	0.81	0.81	2.09
2D- PA-9	0.85	0.85	0.79	2.03
1D-PA-16	0	0.87	0.89	2.19
2D-PA-16	1.31	0.81	0.83	2.05
1D-PA-25	0	1.0	1.0	2.37
2D-PA-25	2.07	2.07	1.77	2.79
1D-PA-36	1.18	1.24	1.24	2.67
2D-PA-36	3.04	8.95[a]	8.97[a]	3.59 (6.15)[b]
1D-PA-49	2.18	1.60	1.68	3.10
2D-PA-49	3.15	8.98	9.00	4.10 (12.26)[c]
1D-PA-64	3.36	2.24	2.31	3.68
2D-PA-64	3.84	16.09[d]	16.11[d]	4.99 (12.26)[c]
1D-PA-81	4.41	2.07	1.44	4.42
2D-PA-81	4.17	25.2[e]	16.10[d]	5.39 (20.4)[f]
1D-PA-100	5.52	4.33	4.47	5.42
2D-PA-100	4.90	36.3[g]	25.3[e]	5.87 (30.5)[h)]
1D-PA-121	4.50	5.25	5.36	6.51
2D-PA-121	5.61	36.4[g]	25.3[e]	6.34 (30.6)[h]
1D-PA-144	8.49	6.61	6.68	8.00
2D-PA-144	6.70	49.50[i]	36.4[g]	6.32 (42.7)[j]

[a] Sextet state.
[b] Quintet state.
[c] Septet state.
[d] Octet state.
[e] Decaplet state.
[f] Nonet state.
[g] Dodecaplet state.
[h] Undecaplet state.
[i] Tetradecaplet state.
[j] Tridecaplet state.

multireference methods. Thus, for **1D-PA** there is a qualitative agreement between DFT and RAS data. Both methods indicate singlet ground state, however, the calculated singlet-triplet gaps were found much higher for RAS calculations (Tables 2 and 3).

As we mentioned above, the nature of the ground state for **2D-PA** series depends on its size. According to the DFT calculations the ground state of **2D-PA** is singlet up to **2D-PA-25**, and starting from **2D-PA-36** the ground state becomes a high spin state of different multiplicity. RAS calculations qualitatively agree with DFT calculations also indicating high spin ground states for **2D-PA-36**, **2D-PA-64**, **2PDA-100** and **2D-PA-121** (Table 3). For **2D-PA-49** and **2D-PA-81** RAS method predicts triplet to be the ground state, being 3.57 and 7.72 kcal/mol more stable than the corresponding septet and nonet electronic states, respectively.

As seen from Table 3, the high spin ground states are mostly single reference states, the squared CI expansion coefficients for the lowest energy configuration exceeds 0.7 (Table 3) in agreement with low spin contamination of these states at DFT level and therefore their electronic structure can be properly described within DFT framework. RAS relative energies for singlet and triplet states of **2D-PA** also agree reasonably well with those obtained using DFT. Only for **2D-PA-16** and **2D-PA-25** DFT and RAS predict different relative energies for these states (Tables 2 and 3).

4. Conclusions

The difference between 1D and 2D conjugated systems depends on the connection densities in 2D systems. Higher connection density implies greater differences between 1D and 2D electronic structures. The difference between 1D and 2D-PMP is reduced to smaller E_g's, and higher IP's and EA's for 2D-PMP of similar sizes. The ground state is closed shell singlet for both 1D and 2D-PMP. The difference between 1D and 2D-PA is much more striking and mostly related with the nature of the ground states of 2D-PA varying from the single reference singlet to the multireference singlet and to the single reference high spin ground states possessing from 4 to 12 unpaired electrons depending on the size of 2D-PA. Both RAS and DFT calculations confirm the high spin nature of the ground states for large 2D-PA's. On the other hand 1D-PA's have a single reference singlet ground state independent on the size of the oligomer. The higher connection density in 2D-PA affects not only the nature of the ground states but also the E_g's and EA's. E_g drops much more rapidly for 2D-PA with size than for 2D-PMP and EA's of 2D-PA are always lower than those of 1D-PA of the same size due to greater electron repulsion.

Acknowledgements

We acknowledge financial support from the Program to Support Research and Technological Innovation Projects (PAPIIT) (grant IN100215) and we would also like to thank the General Direction of Computing and Information Technologies and Communication of the National Autonomous University of Mexico (DGTIC-UNAM) for the support to use the supercomputer facilities. A. E. Torres gratefully acknowledges Consejo Nacional de Ciencia y Tecnología (CONACyT) for a graduate scholarship (245467) and Reyes Flores would like to thank CONACyT for a Postdoctoral Fellowship (173315).

References

[1] W.A. Little, Phys. Rev. 134 (1964) A1416.
[2] Handbook of Organic Conductive Molecules and Polymers, in: H.S. Nalwa (Ed.), John Wiley & Sons, Chichester, 1997.
[3] Electronic Materials: The Oligomer Approach, in: K. Müllen, G. Wegner (Eds.), Wiley VCH, New York, 1998.
[4] Organic Electronic Materials: Conjugated Polymers and Low Molecular Weight Organic Solids, in: R. Farchioni, G. Grosso (Eds.), Springer, Berlin, 2001.
[5] Electronic Materials: From Silicon to Organics, in: L.S. Miller, J.B. Mullin (Eds.), Plenum Press, New York, 1991.
[6] K.S. Novoselov, A.K. Geim, S.V. Morozov, D. Jiang, Y. Zhang, S.V. Dubonos, I.V. Grigorieva, A.A. Firsov, Science 306 (2004) 669.
[7] R.E. Peierls, Quantum Theory of Solids, Clarendon press, Oxford, 1955.
[8] C.H. Choi, M. Kertesz, A.J. Karpfen, Chem. Phys. 107 (1997) 6712.
[9] J. Roncali, Chem. Rev. 97 (1997) 173.
[10] R.H. Baughman, H. Eckhardt, M.J. Kertesz, Chem. Phys. 87 (1987) 6687.
[11] N. Narita, S. Nagai, S. Suzuki, K. Nakao, Phys. Rev. B 58 (1998) 11009.
[12] K. Tanaka, N. Kosai, H. Maruyama, H. Kobayashi, Synth. Met. 92 (1998) 253.
[13] M. Huzak, M.S. Deleuze, B. Hajgató, J. Chem. Phys. 135 (2011) 104704.
[14] J.-P. Malrieu, G. Trinquier, J. Phys. Chem. A 116 (2012) 8226.
[15] S. Rayne, K. Forest, Comput. Theor. Chem. 976 (2011) 105.
[16] A.E. Torres, S. Fomine, Phys. Chem. Chem. Phys. 17 (2015) 10608.
[17] A.E. Torres, P. Guadarrama, S. Fomine, J. Mol. Model. 20 (2014) 2208.
[18] R. Gutzler, D.F. Perepichka, J. Am. Chem. Soc. 135 (2013) 16585.
[19] S. Grimme, S. Ehrlich, L. Goerigk, J. Comp. Chem 32 (2011) 1456.
[20] TURBOMOLE V6.6 2014, a development of University of Karlsruhe and Forschungszentrum Karlsruhe GmbH, 1989–2007, TURBOMOLE GmbH, since 2007. Available from http://www.turbomole.com.
[21] T.H. Dunning Jr., J. Chem. Phys. 90 (1989) 1007.
[22] R. Ditchfield, W.J. Hehre, J. Pople, J. Chem. Phys. 54 (1971) 724.
[23] P.G. Wenthold, J. Hu, R.R. Squires, W.C. Lineberger, J Am. Chem. Soc. 118 (1996) 475.
[24] L. Goerigk, K. Holger, S. Grimme, Chem. Phys. Chem. 12 (2011) 3421.
[25] M.J. Frisch, et al., Gaussian 09, Revision D.01, Gaussian Inc., Wallingford, 2013.
[26] A.R. Moughal-Shahi, C.J. Cramer, L. Gagliardi, Phys. Chem. Chem. Phys. 11 (2009) 10964.
[27] Y. Zhao, D.G. Truhlar, Theor. Chem. Acc. 120 (2008) 215.
[28] D.S. Huh, S.J. Choe, J. Porphyrins Phthalocyanines 14 (2010) 592.
[29] E.A. Kantchev, T.B. Norsten, M.B. Sullivan, Org. Biomol. Chem. 10 (33) (2012) 6682.
[30] S. Kawuchi, L. Antonov, Y. Okuno, Bulg. Chem. Commun. 46 (Special Issue A) (2014) 228.
[31] C. Wang, J. Zhang, G. Long, N. Aratani, H. Yamada, Y. Zhao, Q. Zhang, Angew. Chem. Int. Ed. 54 (2015) 6292.
[32] G. Natta, G. Mazzanti, P. Corradini, Atti. Acad. Naz. Lincei, Cl. Sci. Fis. Mat. Nat. Rend. 25 (8) (1958) 3.
[33] T. Yamamoto, Y. Hayashi, A. Yamamoto, Bull. Chem. Soc. Jpn. 51 (7) (1978) 2091.
[34] M. Bieri, M.-T. Nguyen, O. Gröning, J. Cai, M. Treier, K. Aït-Mansour, K.P. Ruffieux, C.A. Pignedoli, D. Passerone, M. Kastler, K. Müllen, R. Fasel, J. Am. Chem. Soc. 132 (2010) 16669.

[35] B.C. Lin, C.P. Cheng, Z.P.M. Lao, J. Phys. Chem. A 107 (2003) 5241.
[36] M. Malagoli, J.L. Brédas, Chem. Phys. Lett. 327 (2000) 13.
[37] K. Sakanoue, M. Motoda, M. Sugimoto, S. Sakaki, J. Phys. Chem. A 103 (1999) 5551.
[38] S.S. Zade, M. Bendikov, Chem. Eur. J. 14 (2008) 6734.
[39] T.C. Chung, A. Feldblum, A.J. Heeger, A.G. MacDiarmid, J. Chem. Phys. 74 (1981) 5504.
[40] A.A. Ovchinnikov, Theoret. Chim. Acta. (Berl.) 47 (1978) 297.
[41] G. Trinquier, N. Suaud, Jean-Paul Malrieu, Chem. Eur. J. 16 (2010) 8762.
[42] W.L. Wang, S. Meng, E. Kaxiras, Nano Lett. 8 (1) (2008) 241.
[43] O.V. Yazyev, W.L. Wang, S. Meng, E. Kaxiras Nano Lett. 8 (2) (2008) 766.
[44] H.S. Nalwa (Ed.), Handbook of Advanced Electronic and Photonic Materials and Devices, vol. 1, Academic Press, 2016.